energies

MDPI

Article

Preparation of Hierarchical Porous Carbon from Waterweed and Its Application in Lithium/Sulfur Batteries

Chunyong Liang [1], Xiaomin Zhang [1], Yan Zhao [1,*], Taizhe Tan [2], Yongguang Zhang [1,*] and Zhihong Chen [3,*]

1 School of Materials Science & Engineering, Research Institute for Energy Equipment Materials, Hebei University of Technology, Tianjin 300130, China; liangchunyong@126.com (C.L.); zxm15510922072@163.com (X.Z.)
2 Synergy Innovation Institute of GDUT, Heyuan 517000, China; taizhetan@gdut.edu.cn
3 Shenyang Institute of Automation, Guangzhou, Chinese Academy of Sciences, Guangzhou 511458, China
* Correspondence: yanzhao1984@hebut.edu.cn (Ya.Z.); yongguangzhang@hebut.edu.cn (Yo.Z.); chenzhihong1227@sina.com (Z.C.); Tel.: +86-22-60201447 (Yo.Z.)

Received: 20 April 2018; Accepted: 7 June 2018; Published: 13 June 2018

Abstract: A nanostructured carbon (NSC) material with a hierarchical porous structure is synthesized through the carbonization of a waterweed, namely Echinodorus amazonicus Rataj. The fabricated NSC is used as an electrode material for sulfur of lithium/sulfur (Li/S) batteries. The NSC provides for a high pore volume (0.19 cm^3 g^{-1}) and large specific surface area (111.25 m^2 g^{-1}). Because of the highly hierarchical porous structure of the NSC material, allowing polysulfides to remain in the carbon framework after cycling, the sulfur/NSC composite exhibits an excellent electrochemical performance.

Keywords: nanostructured carbon; hierarchical porous structure; lithium/sulfur batteries; polysulfides

1. Introduction

With the increasing environmental problems caused by conventional energy sources and the gradual depletion of oil resources, clean energy is becoming an important topic for the whole world. As an electrochemical energy storage device, lithium-ion batteries represent the most advanced energy storage technology and are a key solution for powering portable electronics. Despite this, the current performance of lithium-ion batteries is struggling to meet the market requirements and is approaching its theoretical capacity limit [1–6]. Sulfur, as a cathode of lithium/sulfur (Li/S) batteries, possesses a high theoretical specific capacity (1675 mAh g^{-1}) and a high theoretical energy density (2600 Wh kg^{-1}), for this reason, it has aroused great interest [7–10].

However, because of the different reaction mechanisms, Li/S batteries need to be developed in a different way with respect to lithium-ion batteries [11]. One of the main limitations comes from the electronic nature of sulfur, which is commonly referred to as a poor electronic conductor ($\sigma = 5 \times 10^{-30}$ S cm^{-1}) requiring the addition of a conductive element such as carbon. The second problem is that the polysulfide ions formed during the discharge/charge processes tend to dissolve into the organic solvent electrolyte [12]. The diffusion of dissolved polysulfides between the electrodes gives rise to a shuttle effect that results in a severe loss of capacity and Coulombic efficiency upon cycling [13–15].

Many previous investigations have pointed out that porous sulfur/carbon composites can efficiently increase the sulfur uptake and the cycle stability [16–22]. Porous carbon can provide for a good electrical conductivity together with a large pore volume that can effectively relieve the

stress due to the high volume expansion of sulfur cathodes during cycling [23,24]. Current methods for preparing porous carbons are based on laser etching [25], arcs [26], nano-casting [27,28], and others; however, most of these methods are costly and difficult to upscale. For this reason, biomass waste would be an ideal precursor for Li/S battery electrode materials due to the tunable physical and chemical properties, low production cost, and by being a renewable, natural, and environmental friendly resource [29–33].

Aquatic plants, thanks to their luxuriant foliage, rapid growth, low-cost, and high content of carbon species are ideal and sustainable precursors for producing porous biochar. Waterweed, such as Echinodorus amazonicus Rataj (EAR) was shown to possess a highly porous structure and excellent adsorption properties; this has motivated us to select the nanostructured EAR as carbon precursor to synthesize a porous carbon material. Because of its unique hierarchical nanostructure, the resulting nanostructured carbon (NSC) could promote good electrical contact and effectively inhibit the dissolution of polysulfides. The electrochemical performance of the sulfur/NSC (S/NSC) composite as a cathode material for Li/S batteries has also been investigated.

2. Materials and Methods

2.1. Sample Preparation

The NSC material was synthesized following a simple method based on the carbonization of the sole EAR (Lianyungang Yuanhai Garden Technology, Lianyungang, China) carbon precursor and the process was shown in Figure 1. Firstly, EAR was thoroughly cleaned and dried, then the compound was heated at 800 °C with a heating rate of 5 °C min^{-1} and the temperature maintained for 2 h in an argon atmosphere. Then, it was cooled to room temperature, taken out and ground until the formation of a black powder. Then, the powder was dispersed in potassium hydroxide (KOH, Tianjin Guangfu, Tianjin, China, ≥99% purity) solution (1 M) and stirred until the solvent was completely evaporated; then, the powder was heated again at 800 °C for 2 h and cooled down naturally. The KOH residuals were removed by hydrochloric acid (HCl, Tianjin Fuchen, Tianjin, China, ≥99% Purity) and distilled water. Finally, the sample was dried in a drying oven to obtain a chemically activated porous carbon. The S/NSC composite material was obtained by mixing carbon and sulfur (Tianjin Kewei, Tianjin, China, ≥98% purity) in a 1:3 mass ratio, placing the mixture in an autoclave and heating to 155 °C for 10 h [29,34].

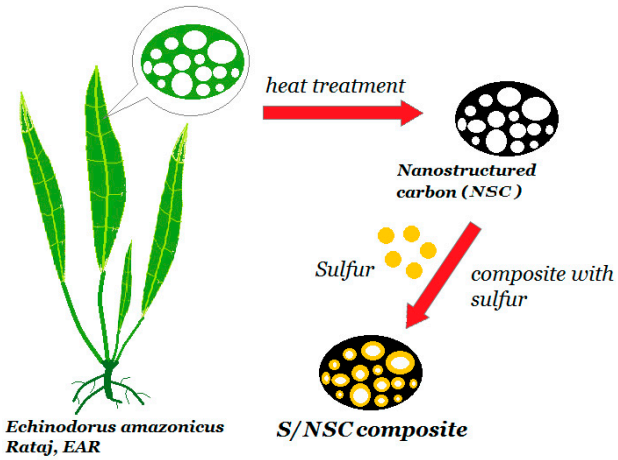

Figure 1. Schematic of the preparation of the sulfur nanostructured carbon (S/NSC).

2.2. Characterization

The infrared spectra were obtained from Fourier transform infrared spectroscopy (FTIR, Thermo Nicolet 6700, Thermo Fisher Scientific, Waltham, MA, USA), the sulfur loading content

was estimated by thermogravimetric analysis (TGA, SDTQ 600) under argon with a heating rate of 5 °C min^{-1} from 25 to 800 °C, the microscopic morphology of the NSC and S/NSC samples was determined by scanning electron microscopy (SEM, S-4800, Hitachi Limited, Tokyo, Japan, equipped with energy dispersive X-ray spectrometry elemental analysis) and transmission electron microscopy (TEM, JEM-2100F, JEOL, Tokyo, Japan), respectively. Raman spectroscopy analysis was performed on Raman spectroscopy (LabRAM Hr 800, HORIBA Jobin Yvon, Paris, France) with a laser wavelength of 514 nm, crystalline structure of the samples were characterized by X-ray diffraction (XRD, Rigaku-TTRIII, Tokyo, Japan) in the range of 10° to 90° at a scan rate of 12° min^{-1}. The surface area was calculated using the Brunauer–Emmett–Teller (BET, ASAP 2020, Micromeritics, Aachen, Germany) equation based on adsorption data and the total pore volume was determined from the amount of nitrogen adsorbed at a relative pressure of 0.98. Pore size distributions (PSDs) were calculated by adsorption isotherms for pores of different sizes. X-ray photoelectron spectroscopy (XPS) analysis was performed on an X-ray photoelectron spectroscopy (XPS, VG ESCALAB MK II, VG Scientific, London, England) at room temperature.

2.3. Cell Fabrication and Electrochemical Measurement

The S/NSC composite, polyvinylidene fluoride (PVDF, Kynar, HSV900), and acetylene black (Shanghai SIMBATT Energy Technology, Shanghai, China, 99.5% purity) were weighted at a mass ratio of 8:1:1 and dissolved in 1-methyl-2-pyrrolidinone (NMP, Sigma-Aldrich, St. Louis, MO, USA, ≥99.5% purity) to obtain the electrode paste, which was coated on aluminum foil (Guangzhou Zhongtian Aluminum Industry, Guangzhou, China) and then dried off. The electrodes were then cut into 1.5 cm diameter sheets and the sulfur loading of the electrode was 2 mg/cm^2. The S/NSC composite was used as the cathode material in a 2025-type coin cell assembled in a glove box filled with argon. The selected electrolyte was tetraethylene glycol dimethyl ether with 1 M lithium trifluoromethanesulfonamide (LiTFSI) (Shenzhen Tianchenghe Technology, Shenzhen, China) [35,36]. Galvanostatic charge/discharge curves were recorded with a multichannel battery tester (BTS-5V5mA, Neware, Shenzhen Xinweier Electronics, Shenzhen, China) between 1.0 and 3.0 V and the capacity was calculated per gram of sulfur. The cyclic voltammetry (CV) and electrochemical impedance spectroscopy (EIS) were measured on a PARSTAT 4000 electrochemical workstation. The cyclic voltammetry (CV) curves were conducted with a scanning rate 0.1 mV s^{-1} between 1.0 and 3.0 V. The impedance spectrums were obtained in the frequency range of 100 kHz to 10 mHz. All the electrochemical measurements were performed at room temperature.

3. Results and Discussion

The FTIR spectra obtained for the NSC and S/NSC samples are shown in Figure 2a. The interaction between C=C and C=N stretching vibrations was observed at 1615 cm^{-1} [37]. Nitrogen-doped carbon is commonly observed in biomass materials because they usually contain a certain amount of proteins; this nitrogen doping can effectively improve the electrochemical performance by chemisorbing from intermediate polysulfides. The absorption peaks at 1473 cm^{-1} and 1428 cm^{-1} are associated with C=C stretching. Compared with NSC, in the S/NSC, we can clearly observe the additional absorption peaks at 1090 cm^{-1} and 669 cm^{-1} associated with the C=S and C-S stretching [38], indicating the chemical bonding between sulfur and NSC. As shown in Figure 2b, there is an abrupt weight loss phase in the TGA curve from the S/NSC composite in the temperature range of 180 to 250 °C. Interestingly, as compared with the initial mass, the weight loss of the S/NSC sample was about 75 wt %, which proves the excellent sulfur incorporation capacity of the NSC, ascribed to its highly porous structure.

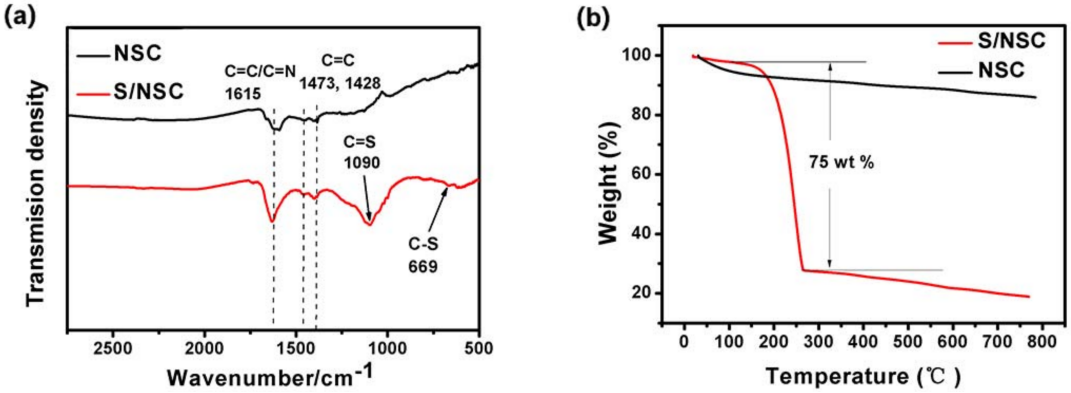

Figure 2. (**a**) Fourier transform infrared spectroscopy (FTIR) spectra of NSC and S/NSC composites; (**b**) thermogravimetric curve of NSC and S/NSC composites.

The scanning electron microscopy analysis was used to characterize the micromorphology of the NSC and S/NSC samples (Figure 3). The 3D connected spongelike structure of the precursor was well preserved without major damages. Moreover, it is found that the NSC is composed of connected flakes with a wrinkled surface. As shown in Figure 3e–g, sulfur was uniformly distributed throughout the carbon framework, proving that sulfur is successfully impregnated into the pores of the NSC. The EDX spectrum analysis is shown in the inset of Figure 3e, showing that the composite material contains both C (30%) and S (70%) elements.

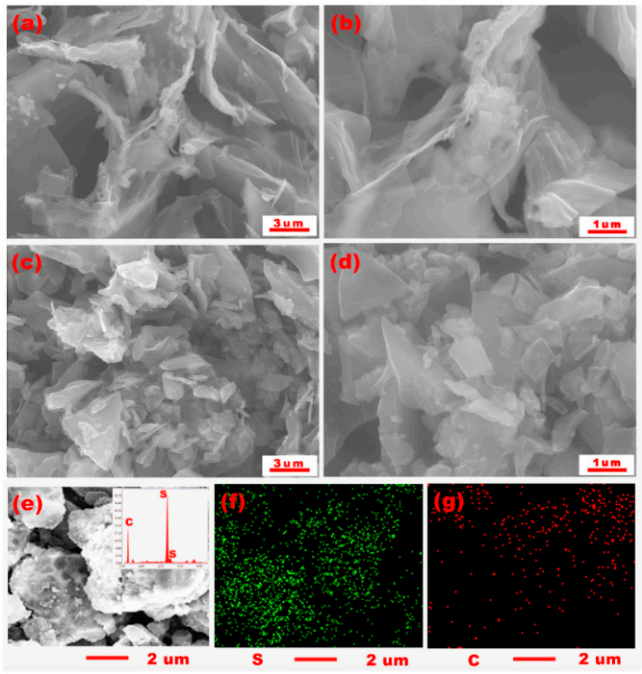

Figure 3. Typical SEM images of (**a**,**b**) NSC, (**c**,**d**) S/NSC composite; (**e**) SEM image of a select region of the S/NSC composite and the element energy spectrum; (**f**,**g**) the element mapping of the S/NSC sample.

High-magnification transmission electron microscopy images clearly show the presence of white spots in the NSC sample (Figure 4a), testifying to the highly porous material structure together with its large specific surface area. The size of white spots in the S/NSC composite is significantly reduced (Figure 4b), indicating that sulfur has partially filled the nanopores of the NSC.

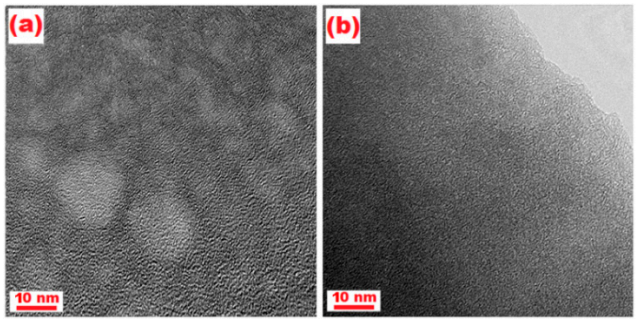

Figure 4. TEM images of sample (**a**) NSC and (**b**) S/NSC.

Raman spectroscopy was used to analyze the molecular structure of the carbon material (Figure 5a). Two peaks at 1360.5 cm^{-1} (D-band) and 1597.4 cm^{-1} (G-band) can be clearly distinguished: The D-band represents disordered carbon of the graphite structure, while the G-band corresponds to the E_{2g} mode (stretching vibrations) of the crystalline graphite [39]. The graphitization degree of the carbon materials was evaluated based on the intensity ratio of the D-band to the G-band (I_D/I_G) [7]: the smaller the ratio, the higher the degree of ordering in the carbon material [40]. In the S/NSC composite, I_D/I_G is almost the same as in the pure porous carbon sample except for the sulfur diffraction peak. We could find it in the range of 700-450 cm^{-1}, where sulfur could obviously be identified. The peak at 486 cm^{-1} could correspond to the S-S bond [41]. This also shows that elemental sulfur was dispersed evenly in the composite. In Figure 5b an exemplary curve fit for the SNC sample was shown. Pöschl et al. proved that in the interpretation of soot Raman spectra, the range 1000–2000 cm^{-1} should be performed with five bands: G, D1 (D), D2, D3, and D4. The G-band is ascribed to the presence of an ideal graphitic lattice, the D, D2, and D4 bands confirm the presence of a disordered graphitic lattice while the D3-band originates from the amorphous carbon phase [42]. X-ray diffraction patterns from the NSC and S/NSC composite samples are shown in Figure 5c, there are broad halos in the range of 20–30 2 theta, indicating carbon with an amorphous structure [43]. The reduction of these sulfur-related crystalline peaks (marked in the picture) upon sulfur uptake indicates that most of the sulfur has impregnated the porous carbon; however, several diffraction peaks related to sulfur on the carbon appear, which demonstrates that some sulfur with a strong crystalline form remains in the composite.

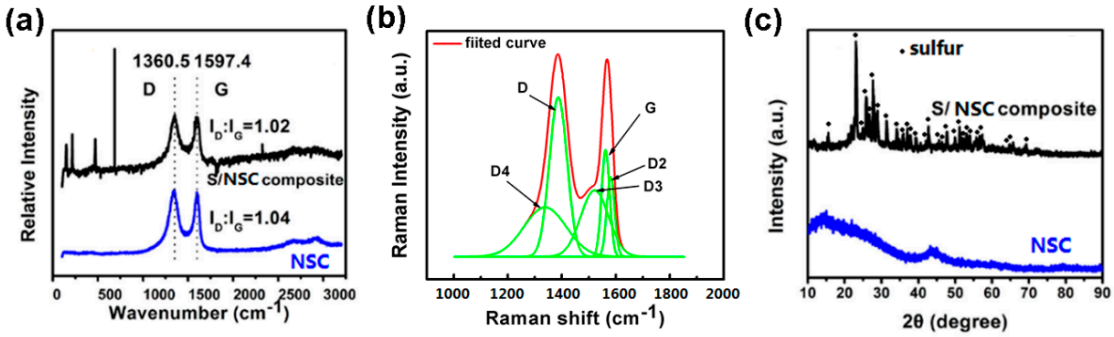

Figure 5. (**a**) Raman spectra (**b**) curve fit for the NSC sample and (**c**) XRD patterns of NSC and S/NSC composites.

The nitrogen adsorption-desorption isotherms of Figure 6 are acquired to evaluate the Brunauer–Emmett–Teller (BET) specific surface area and pore size distribution (PSD) curves of the NSC and S/NSC samples. The adsorption curves correspond to type IV-isotherms, indicating the presence of mesopores; the BET surface area and pore volume in NSC is 111.25 m^2 g^{-1} and 0.19 cm^3 g^{-1}, respectively. The decrease following the sulfur uptake is due to the filling of mesopores of the carbon-based material. Figure 6b indicates that the size of the pores is in the order of a few to tens of

nanometers, it also shows that the activation produced both mesopores and micropores, with a mean size of less than 2 nm (micropores) in the S/NSC sample, confirming that the elemental sulfur has filled the pores.

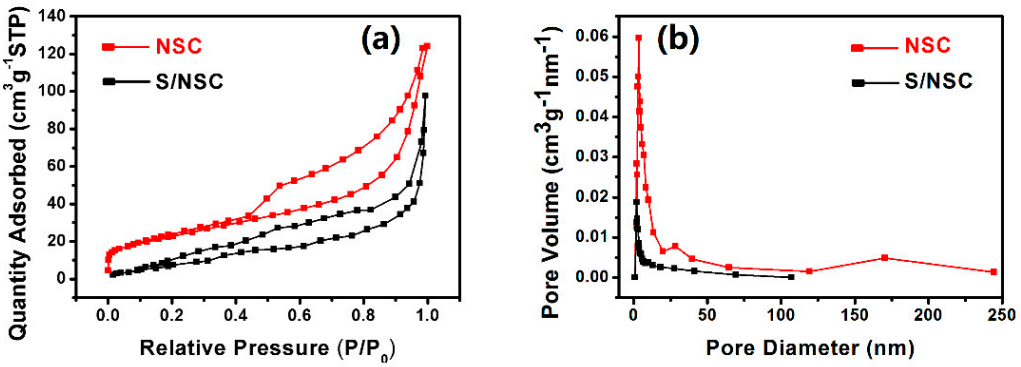

Figure 6. (**a**) N_2 adsorption–desorption isotherms and (**b**) pore diameter distribution of the NSC and the S/NSC composite.

The Survey XPS spectra of S/NSC are shown in Figure 7. The C 1s spectrum of S/NSC was fitted with four peaks centered at 284.4, 285.2, 286.4, and 288.9 eV binding energy, attributed to C-C/C=C, sp^3-C, C-O, and O-C=O bonds [44], respectively (Figure 7c). Among them, the C-S bond, compared to Figure 7b, shows the combination of carbon and sulfur. As shown in Figure 7d, the S 2p spectrum shows five adjacent peaks attributed to S $2P_{3/2}$ (164.2 eV), S-O (164.6 eV), S $2p_{1/2}$ (165.4 eV), S-O (165.8 eV), and S-O (169.2 eV) bonds.

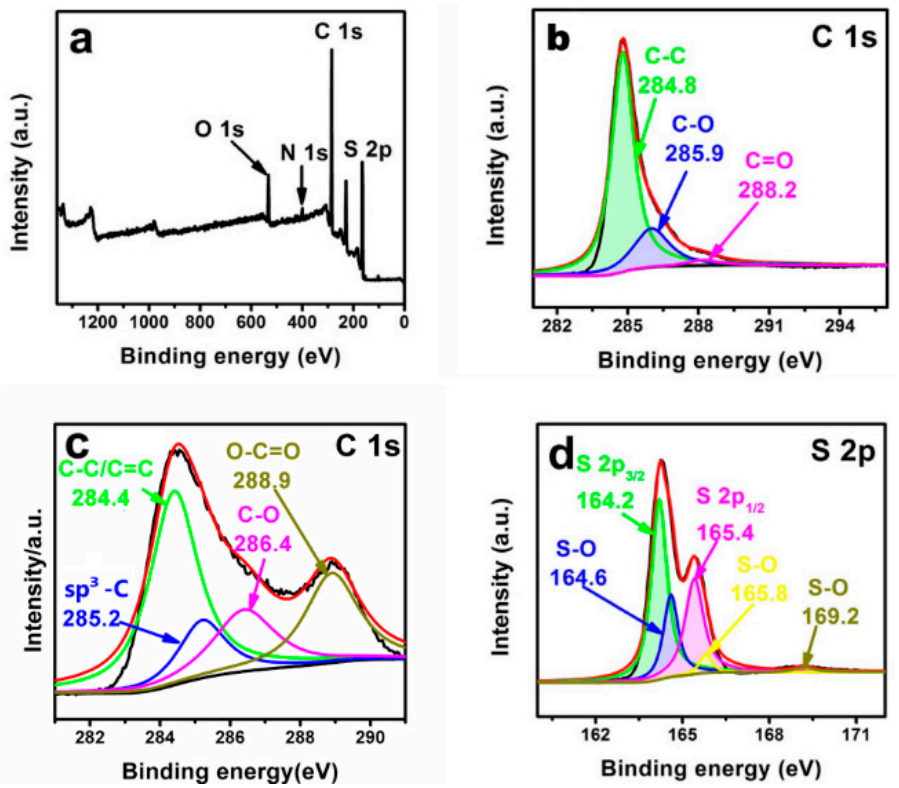

Figure 7. (**a**) Survey XPS spectrum of S/NSC; (**b**) C 1s spectra of NSC composite; (**c**,**d**) C 1s and S 2p spectra of S/NSC sample, respectively.

Figure 8a shows the cyclic voltammograms (CV) of a S/NSC composite electrode for the first two cycles. Two typical plateaus are observed at 2.36 and 2.10 V in the reduction process, related to the reduction of sulfur to soluble higher-order lithium polysulfide (Li_2S_n, $4 \leq n \leq 8$) and soluble lithium polysulfide to insoluble Li_2S_2 and Li_2S, respectively. The charge profiles show the oxidation plateau at 2.45 V, which relates to the reverse reaction during the charge process. Moreover, the first two cycles of the CV curve almost completely coincided, indicating the good cycle performance of the battery.

In the discharge-charge curve (Figure 8b), it can be seen that the platforms were consistent with the position of the peak in this figure. A significant initial specific discharge capacity of 1387.8 mAh g^{-1} at 0.1 C was measured, and the capacity reduced to 938.2 mAh g^{-1} by the 50th cycle, this is due to the loss of sulfur deposited on the surface and the escape of some intermediate soluble polysulfides from the nanopores of the carbon structure [34]. Afterwards, however, the capacity fading rate is considerably lower, there was still 898.2 mAh g^{-1} at 100th cycle, and after 150 cycles, the S/NSC electrode still show a capacity of 823.5 mAh g^{-1}.

As shown in Figure 8c, the coulombic efficiency and cycling performance at 0.1 C of S/NSC composite and carbon black-sulfur composite. Coulombic efficiency is high for both samples, 99% and 98%, respectively, which shows the excellent cycle stability of both batteries. However, there was a large difference in the cycle performance. Compared with the carbon black-sulfur sample, the cycle performance of the S/NSC sample has a great advantage from the initial cycle to the 150th cycle. This result intuitively shows that the addition of the NSC carbon matrix significantly improves the electrochemical performance of the Li-S battery. This is due to the porous structure of the NSC material and its ability to immobilize sulfur and sulfur polysulfides.

Figure 8d shows the rate performance of the S/NSC electrode at the current density from 0.1 C to 1 C (1 C = 1675 mAh g^{-1}). The discharge capacity of the S/NSC is 725.4 mAh g^{-1} at 1 C and it reaches 1043.2 mAh g^{-1} when the current density goes back to 0.1 C; this shows that the battery has a great reversibility and rate performance. In a related study of biomass materials as a carrier of sulfur for cathode materials of lithium-sulfur batteries, this result is very competitive. For example, in the study of Yang's group, they used an apricot shell as a carrier of sulfur, and the initial discharge specific capacity of the battery was 1277 mAh g^{-1} [45]. Moreover, the rate performance of S/NSC is also significantly better than that of Qu's group. They used biomass waste (gelatin) as a carbon-based material for lithium-sulfur battery cathodes [46]. Obviously, the porous structure of NSC material provides for a high encapsulation ability of sulfur particles, which confers to the battery its good electrochemical performance.

As shown in Figure 8e, the EIS spectra of the S/NSC electrode after first and forth cycles show typical Nyquist plots, comprising a compressed semicircle in the high to medium frequency range and an inclined line in the low frequency range; the semicircle at high-middle frequency is attributed to the charge-transfer resistance. The inclined line in the low-frequency region refers to the Warburg impedance [47]. It can be seen that after four cycles the Nyquist plot of the cell has transformed from a single compressed semicircle type to two compressed semicircles. This transition indicates that an interfacial change occurred during the discharge/charging process, which protected the cathode from further decomposition, indicating the good cycle stability of the battery [32].

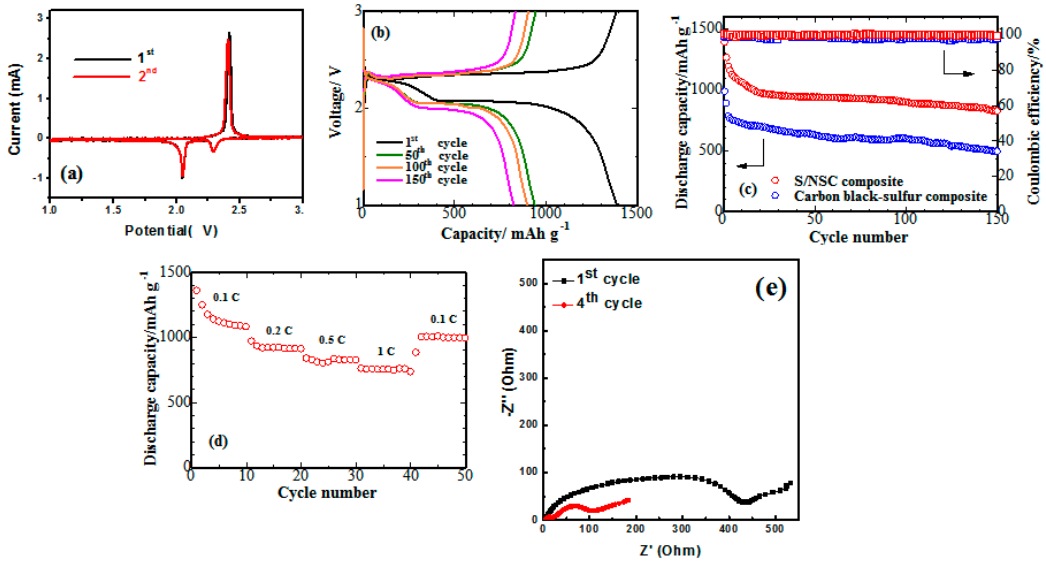

Figure 8. (**a**) CV curves of battery at a scan rate of 0.1 mV s^{-1}; (**b**) discharge/charge performance of battery at 0.1 C; (**c**) cycling performance and coulombic efficiency at 0.1 C of S/NSC composite and carbon black-sulfur composite; (**d**) rate performance of the S/NSC battery at various current densities; (**e**) Nyquist plots of the S/NSC electrode at first and forth cycle.

In order to determine the distribution of the electrode material elements after the cycle, we scanned the electrode after 150 charge/discharge cycles. As shown in Figure 9, after the charge and discharge cycles, the sulfur and carbon element remained in a uniformly distributed state. This phenomenon supports the argument that the recycled sulfur remains in the carbon structure, indicating that the NSC porous carbon material we prepared indeed has a good sulfur-retaining capacity. It provides strong support for its good electrochemical performance.

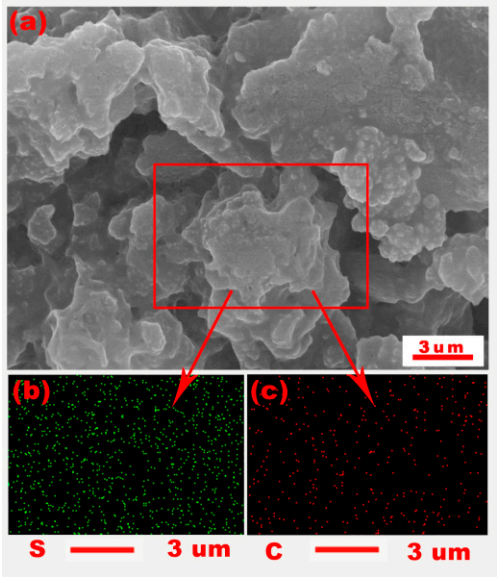

Figure 9. (**a**) SEM images of the S/NSC composite electrode after 150 cycles and (**b**,**c**) the element mapping of the selected region of electrode.

4. Conclusions

In summary, we used a low-cost biomass material, processed by a simple method, as the cathode material for lithium-sulfur batteries and achieved good results. The nanostructured carbon was synthesized by carbonizing Echinodorus amazonicus Rataj and the S/NSC composite was prepared by the melt diffusion method. The hierarchical porous structure of the NSC balanced the volume expansion of sulfur in electrochemical reactions, which confers to the material a strong polysulfide constraining ability; the S/NSC composite was applied as a cathode material for lithium/sulfur batteries showing a high discharge capacity and excellent cycling stability.

Author Contributions: Formal analysis, C.L. and T.T.; Investigation, X.Z.; Project administration, Y.Z. (Yan Zhao) and Y.Z. (Yongguang Zhang); Supervision, Y.Z. (Yan Zhao), Y.Z. (Yongguang Zhang) and Z.C.; Writing-original draft, C.L.; Writing-review & editing, Y.Z. (Yan Zhao) and Z.C.

Acknowledgments: This work was supported by the Program for the Outstanding Young Talents of Hebei Province; Guangdong Provincial Science and Technology Project (2017A050506009).

Conflicts of Interest: The authors declare no conflict of interest.

References

1. Zhao, L.; Hu, Y.S.; Li, H.; Wang, Z.; Chen, L. Porous $Li_4Ti_5O_{12}$ Coated with N-Doped Carbon from Ionic Liquids for Li-Ion Batteries. *Adv. Mater.* **2011**, *23*, 1385–1388. [CrossRef] [PubMed]
2. Półrolniczak, P.; Nowicki, P.; Wasiński, K.; Pietrzak, R.; Walkowiak, M. Biomass-derived hierarchical carbon as sulfur cathode stabilizing agent for lithium-sulfur batteries. *Solid State Ion.* **2016**, *297*, 59–63. [CrossRef]
3. Yang, Z.; Zhang, J.; Kintnermeyer, M.C.; Lu, X.; Choi, D.; Lemmon, J.P.; Liu, J. Electrochemical energy storage for green grid. *Chem. Rev.* **2011**, *111*, 3577–3613. [CrossRef] [PubMed]
4. Etacheri, V.; Marom, R.; Elazari, R.; Salitra, G.; Aurbach, D. Challenges in the development of advanced Li-ion batteries: A review. *Energy Environ. Sci.* **2011**, *4*, 3243–3262. [CrossRef]
5. Zhang, Y.G.; Li, Y.; Li, H.P.; Yin, F.X.; Zhao, Y.; Bakenov, Z. Synthesis of hierarchical MoS_2 microspheres composed of nanosheets assembled via facile hydrothermal method as anode material for lithium-ion batteries. *J. Nanopart. Res.* **2016**, *18*, 1–9. [CrossRef]
6. Li, H.P.; Li, Y.; Zhang, Y.G.; Zhang, C.W. Facile synthesis of carbon-coated Fe_3O_4 core–shell nanoparticles as anode materials for lithium-ion batteries. *J. Nanopart. Res.* **2015**, *17*, 1–9. [CrossRef]
7. Zhu, Y.; Xu, G.Y.; Zhang, X.L.; Wang, S.J.; Li, C.; Wang, G.X. Hierarchical porous carbon derived from soybean hulls as a cathode matrix for lithium-sulfur batteries. *J. Alloys Compd.* **2017**, *695*, 2246–2252. [CrossRef]
8. Bruce, P.G.; Hardwick, L.J.; Abraham, K.M. Lithium-air and lithium-sulfur batteries. *MRS Bull.* **2011**, *36*, 506–512. [CrossRef]
9. Chen, S.; Huang, X.; Sun, B.; Zhang, J.; Liu, H.; Wang, G. Multi-shelled hollow carbon nanospheres for lithium-sulfur batteries with superior performances. *J. Mater. Chem. A* **2014**, *2*, 16199–16207. [CrossRef]
10. Zhang, Y.G.; Zhao, Y.; Bakenov, Z.; Konarov, A.; Chen, P. Preparation of novel network nanostructured sulfur composite cathode with enhanced stable cycle performance. *J. Power Sources* **2014**, *270*, 326–331. [CrossRef]
11. Barchasz, C.; Leprêtre, J.C.; Alloin, F.; Patoux, S. New insights into the limiting parameters of the Li/S rechargeable cell. *J. Power Sources* **2012**, *199*, 322–330. [CrossRef]
12. Scheers, J.; Fantini, S.; Johansson, P. A review of electrolytes for lithium-sulphur batteries. *J. Power Sources* **2014**, *255*, 204–218. [CrossRef]
13. Feng, X.; Song, M.K.; Stolte, W.C.; Gardenghi, D.; Zhang, D.; Sun, X.; Zhu, J.; Cairns, E.J.; Guo, J. Understanding the degradation mechanism of rechargeable lithium/sulfurcells: A comprehensive study of sulfur-graphene oxide cathode after discharge-charge cycling. *Phys. Chem. Chem. Phys.* **2014**, *16*, 16931–16940. [CrossRef] [PubMed]
14. Mikhaylik, Y.V.; Akridge, J.R. Polysulfide shuttle study in the Li/S battery system. *J. Electrochem. Soc.* **2004**, *151*, A1969–A1976. [CrossRef]
15. Zhang, Q.; Wang, Y.; Seh, Z.W.; Fu, Z.; Zhang, R.; Cui, Y. Understanding the anchoring effect of two-dimensional layered materials for lithium-sulfur batteries. *Nano Lett.* **2015**, *15*, 3780–3786. [CrossRef] [PubMed]

16. Lin, Z.; Liu, Z.; Dudney, N.J.; Liang, C. Lithium superionic sulfide cathode for all-solid lithium-sulfur batteries. *ACS Nano* **2013**, *7*, 2829–2833. [CrossRef] [PubMed]
17. Li, X.; Rao, M.; Lin, H.; Chen, D.; Liu, Y.; Liu, S.; Liao, Y.; Xing, L.; Xu, M.; Li, W. Sulfur loaded in curved graphene and coated with conductive polyaniline: Preparation and performance as a cathode for lithium-sulfur batteries. *J. Mater. Chem. A* **2015**, *3*, 18098–18104. [CrossRef]
18. Li, H.P.; Sun, L.C.; Zhang, Y.G.; Tan, T.Z.; Wang, G.K.; Bakenov, Z. Enhanced cycle performance of Li/S battery with the reduced graphene oxide/activated carbon functional interlayer. *J. Nat. Gas. Chem.* **2017**, *6*, 1276–1281. [CrossRef]
19. Zhou, X.; Chen, F.; Yang, J. Core@shell sulfur@polypyrrole nanoparticles sandwiched in graphene sheets as cathode for lithium-sulfur batteries. *J. Energy Chem.* **2015**, *24*, 448–455. [CrossRef]
20. Wang, C.; Chen, H.; Dong, W.; Ge, J.; Lu, W.; Wu, X.; Guo, L.; Chen, L. Sulfur-amine chemistry-based synthesis of multi-walled carbon nanotube-sulfur composites for high performance Li-S batteries. *Chem. Commun.* **2014**, *50*, 1202–1204. [CrossRef] [PubMed]
21. Zhou, X.; Chen, F.; Yang, J.; Ma, L.; Bai, T.; Long, B.; Liao, Q.; Liu, C. Dual protection of sulfur by interconnected porous carbon nanorods and graphene sheets for lithium-sulfur batteries. *J. Electroanal. Chem.* **2015**, *747*, 59–67. [CrossRef]
22. Li, X.; Rao, M.; Chen, D.; Lin, H.; Liu, Y.; Liao, Y.; Xing, L.; Li, W. Sulfur supported by carbon nanotubes and coated with polyaniline: Preparation and performance as cathode of lithium-sulfur cell. *Electrochim. Acta* **2015**, *166*, 93–99. [CrossRef]
23. Yang, J.; Wang, S.; Ma, Z.; Du, Z.; Li, C.; Song, J.; Wang, G.; Shao, G. Novel nitrogen-doped hierarchically porous coralloid carbon materials as host matrixes for lithium-sulfur batteries. *Electrochim. Acta* **2015**, *159*, 8–15. [CrossRef]
24. Zhao, Y.; Yin, F.X.; Zhang, Y.G.; Zhang, C.W.; Mentbayeva, A.; Umirov, N.; Xie, H.X.; Bakenov, Z. A Free-Standing Sulfur/Nitrogen-Doped Carbon Nanotube Electrode for High-Performance Lithium/Sulfur Batteries. *Nanoscale Res. Lett.* **2015**, *10*, 1–6. [CrossRef] [PubMed]
25. Smalley, R.E. Crystalline ropes of metallic carbon nanotubes. *Science* **1996**, *273*, 483–487.
26. Journet, C.; Maser, W.K.; Bernier, P.; Loiseau, A.; Chapelle, M.L.D.L.; Lefrant, S.; Deniard, P.; Lee, R.; Fischer, J.E. Large-scale production of single-walled carbon nanotubes by the electric-arc technique. *Nature* **1997**, *388*, 756–758. [CrossRef]
27. Liu, M.; Gan, L.; Tian, C.; Zhu, J.; Xu, Z.; Hao, Z.; Chen, L. Mesoporous carbon foams through surfactant templating. *Carbon* **2007**, *45*, 3045–3046. [CrossRef]
28. Kim, T.W.; Park, I.S.; Ryoo, R. A synthetic route to ordered mesoporous carbon materials with graphitic pore walls. *Angew. Chem.* **2003**, *42*, 4375–4379. [CrossRef] [PubMed]
29. Chen, F.; Yang, J.; Bai, T.; Long, B.; Zhou, X.Y. Biomass waste-derived honeycomb-like nitrogen and oxygen dual-doped porous carbon for high performance lithium-sulfur batteries. *Electrochim. Acta* **2016**, *192*, 99–109. [CrossRef]
30. Hernández-Rentero, C.; Córdoba, R.; Moreno, N.; Caballero, A.; Morales, J.; Olivares-Marín, M.; Gómez-Serrano, V. Low-cost disordered carbons for Li/S batteries: A high-performance carbon with dual porosity derived from cherry pits. *Nano Res.* **2018**, *11*, 89–100. [CrossRef]
31. Zhao, Y.; Ren, J.; Tan, T.Z.; Babaa, M.R.; Bakenov, Z.; Liu, N.; Zhang, Y.G. Biomass Waste Inspired Highly Porous Carbon for High Performance Lithium/Sulfur Batteries. *Nanomaterials* **2017**, *7*, 260. [CrossRef] [PubMed]
32. Zhang, Y.G.; Zhao, Y.; Konarov, A.; Li, Z.; Chen, P. Effect of mesoporous carbon microtube prepared by carbonizing the poplar catkin on sulfur cathode performance in Li/S batteries. *J. Alloys Compd.* **2015**, *619*, 298–302. [CrossRef]
33. KalaiSelvan, R.; Zhu, P.; Yan, C.; Zhu, J.D.; Dirican, M.; Shanmugavani, A.; Lee, Y.S.; Zhang, X.W. Biomass-derived porous carbon modified glass fiber separator as polysulfide reservoir for Li-S batteries. *J. Colloid Interface Sci.* **2017**, *513*, 231–239.
34. Wu, H.; Mou, J.; Zhou, L.; Zheng, Q.J.; Jiang, N.; Lin, D.M. Cloud cap-like, hierarchically porous carbon derived from mushroom as an excellent host cathode for high performance lithium-sulfur batteries. *Electrochim. Acta* **2016**, *212*, 1021–1030. [CrossRef]

35. Geng, Z.; Xiao, Q.F.; Wang, D.B.; Yi, G.H.; Xu, Z.G.; Li, B.; Zhang, C.M. Improved Electrochemical Performance of Biomass-Derived Nanoporous Carbon/Sulfur Composites Cathode for Lithium-Sulfur Batteries by Nitrogen Doping. *Electrochim. Acta* **2016**, *202*, 131–139. [CrossRef]
36. Xiang, M.; Wang, Y.; Wu, J.; Guo, Y.; Wu, H.; Zhang, Y.; Liu, H. Natural Silk Cocoon Derived Nitrogen-doped Porous Carbon Nanosheets for High Performance Lithium-Sulfur Batteries. *Electrochim. Acta* **2016**, *227*, 7–16. [CrossRef]
37. Agarwala, U.; Singh, B. Transition metal complexes of 1-substituted tetrazoline-5-thiones. *J. Inorg. Nucl. Chem.* **1969**, *31*, 2515–2525. [CrossRef]
38. Rao, C.N.R.; Venkataraghavan, R.; Kasturi, T.R. Contribution to the Infrared Spectra of Organosulphur Compounds. *Can. J. Chem.* **1964**, *42*, 36–42. [CrossRef]
39. He, C.N.; Wu, S.; Zhao, N.Q.; Shi, C.S.; Liu, E.Z.; Li, J.J. Carbon-Encapsulated Fe_3O_4 Nanoparticles as a High Rate Lithium Ion Battery Anode Material. *Acs Nano* **2013**, *7*, 4459–4469. [CrossRef] [PubMed]
40. Li, J.; Guo, J.Q.; Deng, J.N.; Huang, Y.J. Enhanced electrochemical performance of lithium-sulfur batteries by using mesoporous TiO_2 spheres as host materials for sulfur impregnation. *Mater. Lett.* **2017**, *189*, 188–191. [CrossRef]
41. Van Wart, H.E.; Lewis, A.; Scheraga, H.A.; Saeva, F.D. Disulfide bond dihedral angles from Raman spectroscopy. *Proc. Natl. Acad. Sci. USA* **1973**, *70*, 2619–2623. [CrossRef] [PubMed]
42. Sadezky, A.; Muckenhuber, H.; Grothe, H.; Niessner, R.; Poschl, U. Raman microspectroscopy of soot and related carbonaceous materials: Spectral analysis and structural information. *Carbon* **2005**, *43*, 1731–1742. [CrossRef]
43. Lee, H.M.; Kang, H.R.; An, K.H.; Kim, H.G.; Kim, B.J. Comparative studies of porous carbon nanofibers by various activation methods. *Carbon Lett.* **2013**, *14*, 91–102. [CrossRef]
44. Fan, Y.; Liu, P.F.; Yang, Z.J.; Jiang, T.W.; Yao, K.L.; Han, R.; Huo, X.X.; Xiong, Y.Y. Bi-functional porous carbon spheres derived from pectin as electrode material for supercapacitors and support material for Pt nanowires towards electrocatalytic methanol and ethanol oxidation. *Electrochim. Acta* **2015**, *163*, 140–148. [CrossRef]
45. Yang, K.; Gao, Q.; Tan, Y.; Tian, W.; Zhu, L.H.; Yang, C.X. Microporous carbon derived from Apricot shell as cathode material for lithium–sulfur battery. *Microporous Mesoporous Mater.* **2015**, *204*, 235–241. [CrossRef]
46. Qu, Y.H.; Zhang, Z.; Zhang, X.H.; Ren, G.D.; Lai, Y.Q.; Liu, Y.X.; Li, J. Highly ordered nitrogen-rich mesoporous carbon derived from biomass waste for high-performance lithium–sulfur batteries. *Carbon* **2015**, *84*, 399–408. [CrossRef]
47. Martha, S.K.; Markovsky, B.; Grinblat, J. $LiMnPO_4$ as an Advanced Cathode Material for Rechargeable Lithium Batteries. *J. Electrochem. Soc.* **2009**, *156*, 8559–8563. [CrossRef]